Ultra-Microporous Fe-MOF with Exceptional NO Delivery Kinetics in Biological Media for Therapeutic Application

Rosana V. Pinto[# [a,d]], Chen-Chen Cao[# [b,c]], Pengbo Lyu [e,f], Iurii Dovgaliuk,[a] Cheng-Yong Su [c,g], Guillaume Maurin [e], Fernando Antunes[d], João Pires[d], Vânia André[h], Carlos Henriques[h], Antoine Tissot* [b], Moisés L.Pinto* [a] and Christian Serre* [b]

# These authors contributed equally to this work.

[a] Dr. R. V. Pinto, Prof. M. L. Pinto
CERENA. Departamento de Engenharia Química, Instituto Superior Técnico, Universidade de Lisboa, 1049-001 Lisboa, Portugal
E-mail: moises.pinto@tecnico.ulisboa.pt
[b] Dr. C. Cao, Dr. I. Dovgaliuk, Dr. A. Tissot, Dr. C. Serre
Institut des Matériaux Poreux de Paris, Ecole Normale Supérieure, ESPCI Paris, CNRS, PSL University, 75005 Paris, France
E-mail: antoine.tissot@ens.psl.eu / christian.serre@ens.psl.eu
[c] Dr. C. Cao, Prof. C. Su
MOE Laboratory of Bioinorganic and Synthetic Chemistry, Lehn Institute of Functional Materials, School of Chemistry, Sun Yat-Sen University, Guangzhou 510275, China
[d] Dr. R. V. Pinto, Prof. F. Antunes, Prof. J. Pires
CQE -Centro de Química Estrutural, Institute of Molecular Sciences, Departamento de Química e Bioquímica, Faculdade de Ciências, Universidade de Lisboa. Lisboa, Portugal.
[e] Dr. P. Lyu, Prof. G. Maurin
ICGM, Univ. Montpellier, CNRS, ENSCM, Montpellier, France
[f] Dr. P. Lyu
Hunan Provincial Key Laboratory of Thin Film Materials and Devices, School of Materials Science and Engineering, Xiangtan University, Xiangtan 411105, China
[g] Prof. C. Su
State Key Laboratory of Applied Organic Chemistry, Lanzhou University, Lanzhou 730000, China
[h] V. André, Prof. Carlos Henriques
CQE - Centro de Química Estrutural – Instituto Superior Técnico, Universidade de Lisboa. Av. Rovisco Pais, 1049-001 Lisboa, Portugal

Keywords: Iron-MOF; Chemical stability; Nitric oxide; Wound healing; Angiogenesis

Summary paragraph

Nitric oxide (NO), as a key element in the regulation of essential biological mechanisms, presents huge potential as a therapeutic agent in the treatment and prevention of chronic diseases. Metal-organic frameworks (MOFs) with open metal sites are promising carriers for NO therapies but delivering it over an extended period in biological media remains a great challenge due to (i) a fast degradation of the material in body fluids and/or (ii) a rapid replacement of NO by water molecules onto the Lewis acid sites.

Here, we propose an unprecedented NO adsorption mechanism based on a new ultra-narrow pores Fe bisphosphonate MOF, denoted MIP-210(Fe) or Fe(H_2O)(Hmbpa) (Hmbpa = p-xylenediphosphonic acid). In MIP-210(Fe), the coordination of NO through the Fe(III) sites is unusually preferred, replacing the water, and creating a stable interaction with the free H_2O and P-OH groups delimiting the very narrow pores. This, associated with the high chemical stability of the MOF enables a very slow replacement of NO by water molecules in biological media, achieving an extraordinarily extended NO delivery over at least 72 hours, exceeding by far the NO kinetics release reported by others porous materials, paving the way for the development of safe and successful gas therapies.

Main text

The exogenous administration of NO at controlled amounts (pmol to µmol) has been proved to be of therapeutic interest for many applications linked to chronic diseases (cancer therapy, cardiovascular diseases, bacterial infection and wound healing)[1–3]. Recent work[4,5] has unveiled that metal-organic frameworks (MOFs) are among the most suitable scaffolds to carry and release NO since their tunable composition allows the development of stable and biocompatible frameworks that can provide a highly efficient packing of NO and the local delivery of pure NO without leaching undesirable species. The NO adsorption mechanism in MOFs is typically governed by either (i) physisorption or by (ii) chemical-coordination through the open metal sites (OMS) present in the pores (chemisorption)[4,6]. This later NO-coordination mode not only allows the tuning of the NO payload by changing the metal or the concentration of accessible OMS, but also ensures a more stable binding of NO. The release in biological media is mainly triggered by free water or phosphate molecules that replace NO on the OMS owing to their stronger affinity, which, along with the fast degradation that features some MOFs, constricts the release lifetimes to a maximum of 2 hours (reached by MIP-177(Ti)[5]). With these release

windows, MOFs can only be used in therapies that requires short periods of supplementation. For the long-term NO therapies, the only carriers releasing NO from several hours to weeks are composite polymers with molecular NO donors. However, they suffer from long-term instability of the NO carrying compounds and from leaching of the NO donor species, resulting in non-localized NO delivery and in the release of toxic compounds (e.g. N-nitrosoamines)[7].

To address the challenge of long-term NO delivery, we developed a new microporous Fe bisphosphonate comprising H_4mbpa (or p-xylenediphosphonic acid) and iron(III) that accommodates narrow pores and iron oxoclusters with accessible OMS. This led to MIP-210(Fe) (MIP stands for the materials of the Institute of Porous Materials of Paris). Iron(III)-based MOFs are of particular interest for biomedical applications due to their high biocompatibility[8]. Few of them (e.g. MIL-100, MIL-127) have already proven to be good NO carriers but their limited stability also leads to a fast NO release[9]. This motivated us to further explore the construction of phosphonate MOFs as they are known to be significantly more chemically stable compared to their metal carboxylates counterparts due to the higher complexing strength of phosphonates. If a few water stable microporous metal(III or IV) bis, tris or tetra phosphonates MOFs have been reported[10–12], to our knowledge there is not yet any iron(III) phosphonate MOF with accessible OMS to bind guest molecules such as NO. This was likely due either to the presence of Cl counter anions[13] and/or the dense framework using a short organic spacer[14].

Synthesis and structure solution

MIP-210(Fe) was simply obtained by hydrothermal synthesis (see details in Methods), leading to parallelepiped shaped crystals with a uniform size distribution (Fig. S1). The synthesis procedure is environmentally friendly and therefore promising for a future scale-up production. Infrared spectroscopy indicates that the solid contains partially deprotonated H_4mbpa linkers, while EDX analysis evidence that the Fe:ligand ratio in the crystals is 1:1 (Fig. S3 and Tab. S1). MIP-210(Fe), of formula $Fe^{III}(H_2O)[O_3P\text{-}CH_2\text{-}C_6H_4\text{-}CH_2\text{-}PO_3H].H_2O$ (as-synthesized form), crystallizes in a monoclinic space group P2(1)/n with unit-cell parameters of a=5.1440(3)Å, b=10.7106(7)Å, c=21.0654(9)Å and β=93.222(4)°. The asymmetric unit contains one p-xylenediphosphonic acid linker and one Fe(III) cation (Fig. 1). Each linker possesses one fully deprotonated phosphonate group ($R\text{-}PO_3^{2-}$) coordinated to three adjacent Fe(III) cations and one partially deprotonated phosphonate group ($R\text{-}HPO_3^{-}$) coordinated to two adjacent Fe(III) cations. On the other hand, Fe(III) cations are surrounded by 5 oxygen

atoms from 5 different phosphonate linkers and by one oxygen atom from a coordinated water molecule, leading to a pseudo-octahedral geometry. These coordination modes give rise to double chains of Fe(III) along the *a* axis that are linked through the phosphonate linker. In addition, the structure, although being non porous to N_2 at 77K, presents ultra-microporous corrugated channels along the *a* axis that contain one terminal water molecule per Fe(III) cation in its pristine form (Fig. 1). The simulated PXRD pattern of the crystal structure corresponds perfectly with the corresponding experimental data, which confirms the purity of the synthesized powder (Fig. S4 and S5, Table S2). In addition, variable temperature PXRD indicated that the framework can hold over 250°C, in agreement with thermogravimetric analysis (Fig. S6 and S7) and that slight but reversible changes appeared around 150°C due to the removal of the physisorbed water molecules (Fig. S8).

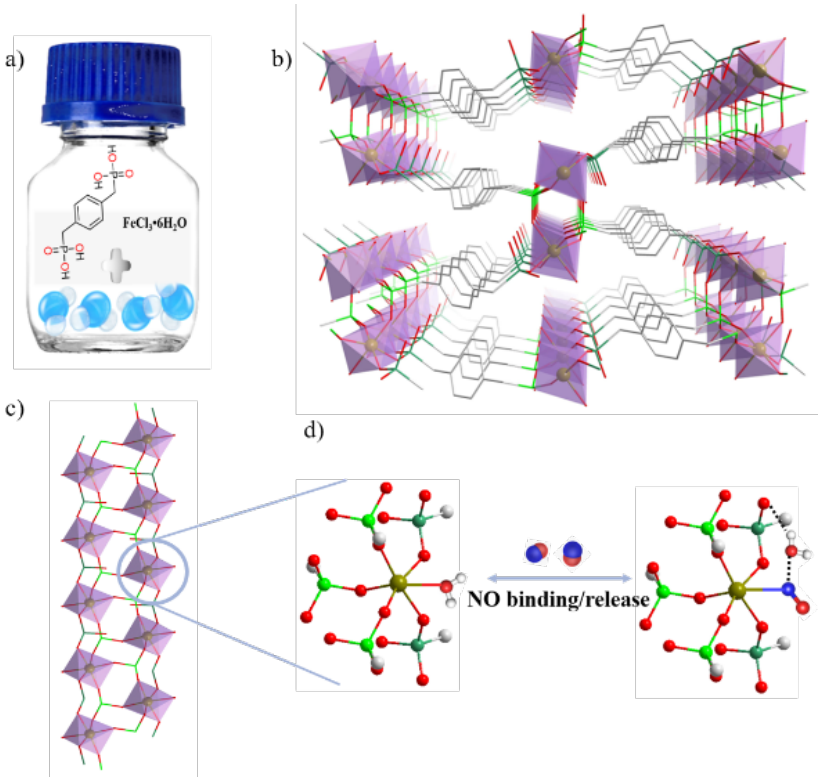

Figure 1. a) Scheme of the synthesis protocol. b) Microporosity of MIP-210(Fe) viewed along the a-axis. c) FeO_6 chain in MIP-210(Fe) and d) illustration of the NO loading/delivery mechanism. Color key: dark yellow, Fe; red, oxygen; gray, carbon; sea/bright green, phosphorus; white, hydrogen. Hydrogen atoms on the MOF framework and non-coordinated guest molecules have been omitted for clarity.

NO adsorption mechanism

NO adsorption measurements on MIP-210 at 80 kPa were carried out after activating the solid at different temperatures to maximize the NO loading (detailed discussion in Supplementary Information – Section 2). MOF activated at 120°C under vacuum (allowing the removal of only physiosorbed water molecules) led to a significant adsorption capacity of 1.86 mmol·g^{-1} after 3 days (Fig. 2A). Surprisingly, higher activation temperatures, associated with the removal of both free and coordinated water molecules led to a contraction of the pores, blocking the diffusion of NO and therefore leading to lower adsorption capacities (Fig. S16). Nonetheless, the adsorption kinetics was found to be rather slow, most likely due to the slow diffusion into the narrow pores, suggesting an incomplete NO loading even after 70 h. The amount adsorbed lies in the range of the reported MOFs studied for NO application (0.8 - 7 mmol·g^{-1})[15–17], with a slightly lower capacity compared to other MOFs presenting Fe open metal sites (i.e. Fe-MIL-100, Fe-MIL-127 and Fe-MIL-88-A with 4.5 mmol·g^{-1}, 2.2 mmol·g^{-1}, 2.5 mmol·g^{-1} NO adsorption capacities, respectively)[9,18], as a consequence of the lower number of OMS in MIP-210 (theoretical amount ~ 3 mmol·g^{-1}).

The desorption curve under vacuum in Fig. 2B showed an initial release in the first 2 hours (ca. 50% of the adsorbed NO) and a very slow delivery after that period. After 24 hours under primary vacuum, ca. 0.56 mmol·g^{-1} (*i.e.,* 30% of the adsorbed NO) remains inside the material, indicating a strong NO adsorption, which is beneficial for a higher control of the therapeutic release and for a safer storage of the loaded material.

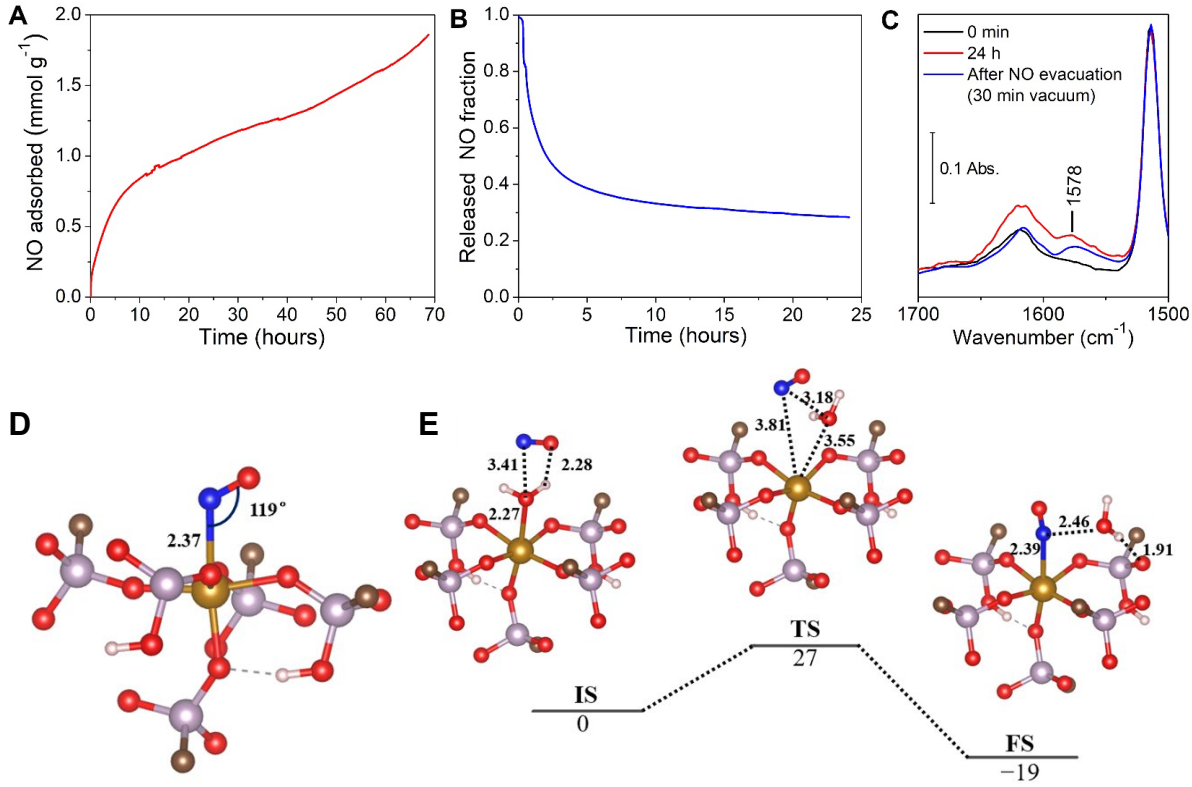

Figure 2. Adsorption studies at 25 °C for NO on MIP-210(Fe) and representation of the NO adsorption mechanism. A) NO adsorption profile performed on a gravimetric apparatus, with 80 kPa NO; B) NO desorption isotherm under high vacuum and C) IR spectra of MIP-210 (previously activated at 120 °C for 12 hours under vacuum), followed by 24 hours of NO exposure at room temperature (1.3 kPa) and its evacuation (30 minutes of vacuum). D and E) Periodic DFT-calculated potential energy profile of the adsorption of NO in MIP-210(Fe) containing initially coordinated water molecule using climbing image nudged elastic band (CI-NEB)[19] method. Color codes: carbon (dark brown), hydrogen (white), oxygen (red), phosphorus (purple), nitrogen (blue) and iron (light brown). The distances and energies are in Å and kJ mol^{-1}, respectively. For sake of clarity only one inorganic node of the periodic structure is shown.

To shed light on the NO adsorption mechanism in MIP-210, *in situ* FTIR studies were first conducted. IR spectra (Fig. 2C) evidence the appearance of a NO adsorption band at 1578 cm^{-1} after 24 hours of exposure to NO, which intensity increased with time (Fig. S15) as a consequence of the slow NO adsorption profile (Fig. 2A). Surprisingly, no band was developed at ca. 1900 cm^{-1}, which is typically assigned to physisorbed NO (i.e. weak interaction of NO)[18]. Thus, we can assume that only chemisorption occurs with the replacement of the coordinated water molecule by NO, which is the most favorable adsorption mechanism for NO therapeutic delivery applications. After 30 minutes under high vacuum, despite losing some intensity, the

band formed at 1578 cm^{-1} persisted, confirming the strong stability of the adsorbed NO species, in agreement with the gravimetric desorption studies (Fig. 2B) that showed a significant NO retention in the solid. Of note, the IR adsorption band observed in MIP-210(Fe) after NO sorption did not match with the band assigned to the NO coordinated on Fe sites (ca. 1800 cm^{-1}) observed in the previously studied Fe-based MOFs for NO adsorption (*i.e.* MIL-100, MIL-127, MIL-88)[9,18]. According to Hadjiivanov[20], bands formed between 1650-1480 cm^{-1} are indicative of the formation of nitrate (NO_3^-) compounds. However, NO_3^- is not likely to form here because NO cannot react with H_2O solely. To get more insights on the consequences of NO adsorption on the MIP-210(Fe) crystalline structure, in situ-PXRD analyses were conducted. After NO being adsorbed, the main Bragg peaks were shifted, in comparison with those of the activated phase (*i.e.* without physiosorbed water in the pores), on the whole similar with the as-synthesized material, in agreement with a filling of the pores (Fig. S17).

Periodic spin-polarized density functional theory (DFT) calculations were further performed to gain atomistic insight into the NO adsorption behavior in MIP-210(Fe). First, we identified that the most stable magnetic configuration of MIP-210(Fe) is an intra-chain anti-ferromagnetic (AFM) state, as shown in Fig. S18 and Table S6. Climbing image nudged elastic band (CI-NEB)[19] method within the Transition State Tools for VASP (VTST)[21] module (see Supplementary Information – Section 2.1 for more details) was further applied to explore the NO adsorption in the MOF encompassing Fe(III) sites coordinated to H_2O to be in line with the activation condition used experimentally before NO adsorption measurement.

As shown in Fig. 2 D and F), H_2O coordinates with Fe with an O-end configuration (Fe-O bond length 2.27 Å) and NO molecule weakly interacts with H_2O molecule via $O(NO)\cdots H(H_2O)$ hydrogen bond (2.28 Å) (initial state IS). Then, the water molecule is released from Fe and Fe-O distance enlarges to 3.55 Å while the NO molecule starts to get close to Fe with Fe-N distance of 3.81 Å in the transition state (TS). In the final state (FS), NO molecule binds to Fe with a Fe-N bond length of 2.39 Å and a Fe-N-O angle of 122°. According to a previous study on N–O stretching frequency of NO molecule within 6-coordinate iron(II) nitrosyl complexes, there is a linear scaling relationship between the Fe-N-O angle and the ν (NO)[22]. While a vibration at 1900 cm^{-1} would correspond to a Fe-N-O angle of 180°, the ν (NO) corresponding to a Fe-N-O angle of 119°should be extrapolated between 1550 and 1600 cm^{-1}, in line with the NO adsorption band at 1578 cm^{-1} observed in the IR spectrum in Fig. 2C. Notably, this NO coordination to Fe(III) is accompanied by rather strong interactions between NO and H_2O (N(NO)-O(H_2O) distance of 2.46 Å) as well as between H_2O and the MOF pore wall (H(H_2O)-O(MOF) distance of 1.91 Å) making this adsorption mode highly stable,

therefore anticipating that a slow release kinetics in water media should be obtained. Further, the overall reaction is exothermic by 19 kJ mol^{-1}, and the activation barrier is only 27 kJ mol^{-1}, which indicates that the H_2O exchange by NO can easily proceed under mild conditions leading to a preferential binding of NO towards Fe(III). The calculations presented in Fig. 2 D and E) were performed considering as a starting point the crystal structure based on the close proximity between the PXRD patterns of the NO loaded sample and the as-synthesized hydrated MOF. A similar trend was obtained considering the crystal structure solved for the material filled with free water molecules (Fig. S19 and Fig. S20), the reaction mechanism being associated with an even lower activation energy barrier (11 kJ mol^{-1}) and being more exothermic (40 kJ mol^{-1}).

NO therapeutic release application. The effectiveness of a vehicle material for NO release is mainly determined by its ability to release NO in a controlled rate, since the NO biological action strongly depends on the available dose (lower or higher values may cause adverse effects) over a certain period. This feature highly depends on how NO is coordinated within the framework and on the accessibility of water present in the biological media towards OMS. As such, quantification of NO released from MIP-210(Fe) was carried out in oxyhemoglobin solution using the oxyhemoglobin assay (Fig. 3), exhibiting an exceptional slow and gradual delivery of NO over at least 70 hours, far beyond the values observed before with the best MOFs or porous inorganic materials. Of note, the stabilization of the conversion in methemoglobin by oxidative reaction between NO and oxyhemoglobin observed at the end of 70 hours may indicate a complete release or a full consumption of the oxyhemoglobin present in the buffer medium. Overall, this method is not able to quantify the complete release profile and consequently the total amount of NO released, but it is very sensitive and demonstrates an initial sustained and very slow NO release rate, as confirmed by the slow conversion to methemoglobin (Fig. 3 inset). Such a slow release is attributed to (i) the previously described unusual NO adsorption mechanism that leads to a strong interaction between NO, the Fe metal sites and the trapped free water molecules inside the narrow pockets of the structure, (ii) the very narrow channels of the MOF and (iii) the high stability of the MOF in several biological media (detailed discussion in Supporting Information – Section 1.3); this considerably slows down the displacement of the coordinated NO by H_2O during the desorption process.

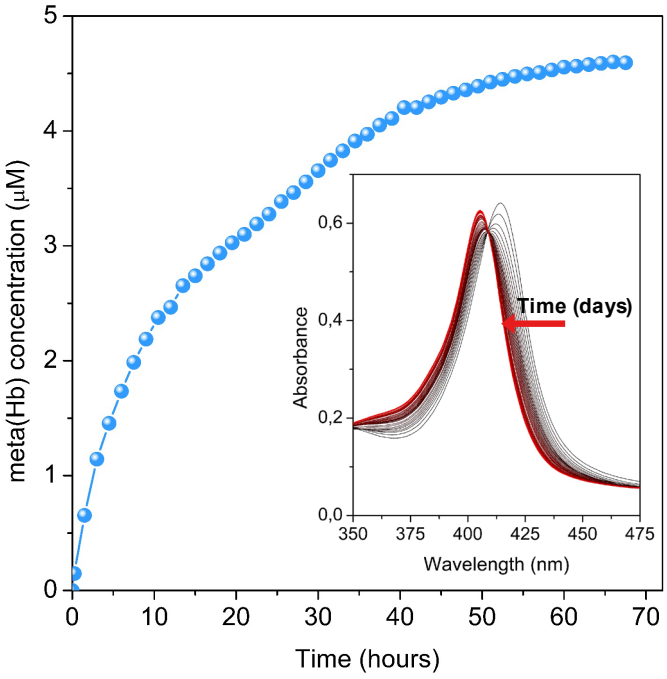

Figure 3. NO release profile from MIP-210 in oxyhemoglobin solution at 25 °C using the oxyhemoglobin quantification assay. Inset depict the changes over 70 hours in the main peak of the oxyhemoglobin-containing solution spectrum, triggered by NO-mediated conversion to methemoglobin.

Before, reported NO-releasing porous materials were limited to a delivery from minutes to few hours due to either fast rehydration and/or degradation of the host solid. For instance, MIP-177(Ti) [5], features a set of suitable properties for such application, including high storage capacity, biocompatibility and stability in biological media, but due to the large pore size, the water diffusion is fast, with a subsequent release of NO that does not last more than 2 hours. On the other hand, zeolites and titanosilicates, that typically are highly stable and biocompatible, present a strong affinity to water that leads to an initial burst of NO release on a duration that never exceeds several minutes[23,24]. The longest release obtained by this class of materials was 4 hours by a modified ETS-4 with copper incorporated in the structure[25]. In addition to its singular release lifetime, MIP-210(Fe) guarantees a sustained release from the beginning, preventing the initial burst of release characteristic in many NO-delivery strategies. Such NO delivery profile is comparable with those obtained by some NO-functionalized polymers and some nanoparticle carriers that already demonstrated therapeutic potential in several pre-clinical studies, encouraging the use of this MOF in numerous biomedical applications[26].

NO released by different concentrations of MIP-210(Fe) did not induce any additional noxious/toxic effect to HeLa and HUVEC cells (Fig. S22-S23), which demonstrates that this controlled release provides a much safer utility of this NO donor in comparison with other compounds. In addition, iron MOFs are expected to be fully biodegradable and poorly toxic even after administration of high doses[27].

After clear evidence of the biocompatibility of MIP-210(Fe) under different cell lines (detailed discussion in Supporting Information – Section 3), first demonstrations of the therapeutic potential of this new NO donor were conducted *in vitro* by performing endothelial migration and tube formation assays. These cellular responses are two pivotal steps in the angiogenesis process, which in turn is critical for many physiologic and pathologic processes such as wound healing and tissue remodeling[28]. The development of new blood vessels is mediated by endothelial cells, which migrate and proliferate in response to growth factors (*e.g.*, vascular endothelial growth factor (VEGF)) to form a functional capillary network[29]. NO is known to significantly contribute to the VEGF mediation and its presence has demonstrated to contribute to an enhanced proliferation and angiogenic response in a concentration-dependent manner[30]. To evaluate the NO-loaded MIP-210(Fe) concentration that triggers the positive biological response, we used the viability assay to compare the effects of unloaded and NO-loaded MIP-210(Fe) at different concentrations. Indeed, the NO released from MIP-210(Fe) should be delivered at low concentrations (nM) to exert an angiogenic effect[31,32]. As discussed in Supporting Information (Section 3), HUVEC viability is affected with MOF concentrations higher than 45 $\mu g.mL^{-1}$. However, at lower MOF concentrations such as 11.75 $\mu g.mL^{-1}$, an enhanced cell viability was observed in presence of NO-loaded MIP-210(Fe) particles compared to cells treated with the NO-free MOF (Fig. S23), which suggests a slight proliferative effect mediated by the released NO. Besides being primary cells, HUVECs are much more sensitive to noxious stimuli than immortalized cells but present a closer behavior to the real systems. For example, HeLa cells show significant resistance to high concentrations of potential toxins[33] and the NO released by MIP-210(Fe) at 900 $\mu g.mL^{-1}$ did not exert any toxic effect on them (Fig. S22).

The ability of NO released by MIP-210(Fe) to induce HUVEC migration was evaluated using a concentration of donor of 11.75 $\mu g.mL^{-1}$, and the effects of NO were compared with the cells treated with unloaded MIP-210(Fe) and with untreated cells. After 24 and 48 hours of treatment, we found that the migration of HUVEC was significantly ($*p<0.05$) faster (*ca.* 8%) compared to the untreated cells and to the cells treated with NO-free MIP-210(Fe) (Fig. 4A and C). To further verify the angiogenic effect of NO, an *in vitro* endothelial tube formation

study employing Geltrex™ as a 3D extracellular matrix was performed. We compared the capillary formation of untreated HUVECs and treated with NO-loaded MIP-210(Fe) and NO-free MIP-210(Fe) after 18 hours at the same NO donor concentration (11.75 $\mu g.mL^{-1}$). Noteworthy, the tube structure of the NO-loaded MIP-210(Fe) group presented a significant richer network (*ca*. 25%) in comparison with the cell control and the NO-free MIP-210(Fe) groups (Fig. 4B and D). An improved migration behavior allows the endothelial cells to migrate faster throughout the wound gap, and a richer capillary formation guarantees the uniform distribution of nutrients, growth factors and functional cells, essential to support the recovery of the full wound[34]. Both cellular responses analyzed here demonstrated that NO is the main contributor of the enhanced migration and tube formation, giving us confidence of the potential angiogenic capacity of the NO-loaded MIP-210(Fe) at the cellular level. To the best of our knowledge, this is the first evidence of the use of a porous solid as a carrier for NO therapeutic pro-angiogenic targeting delivery.

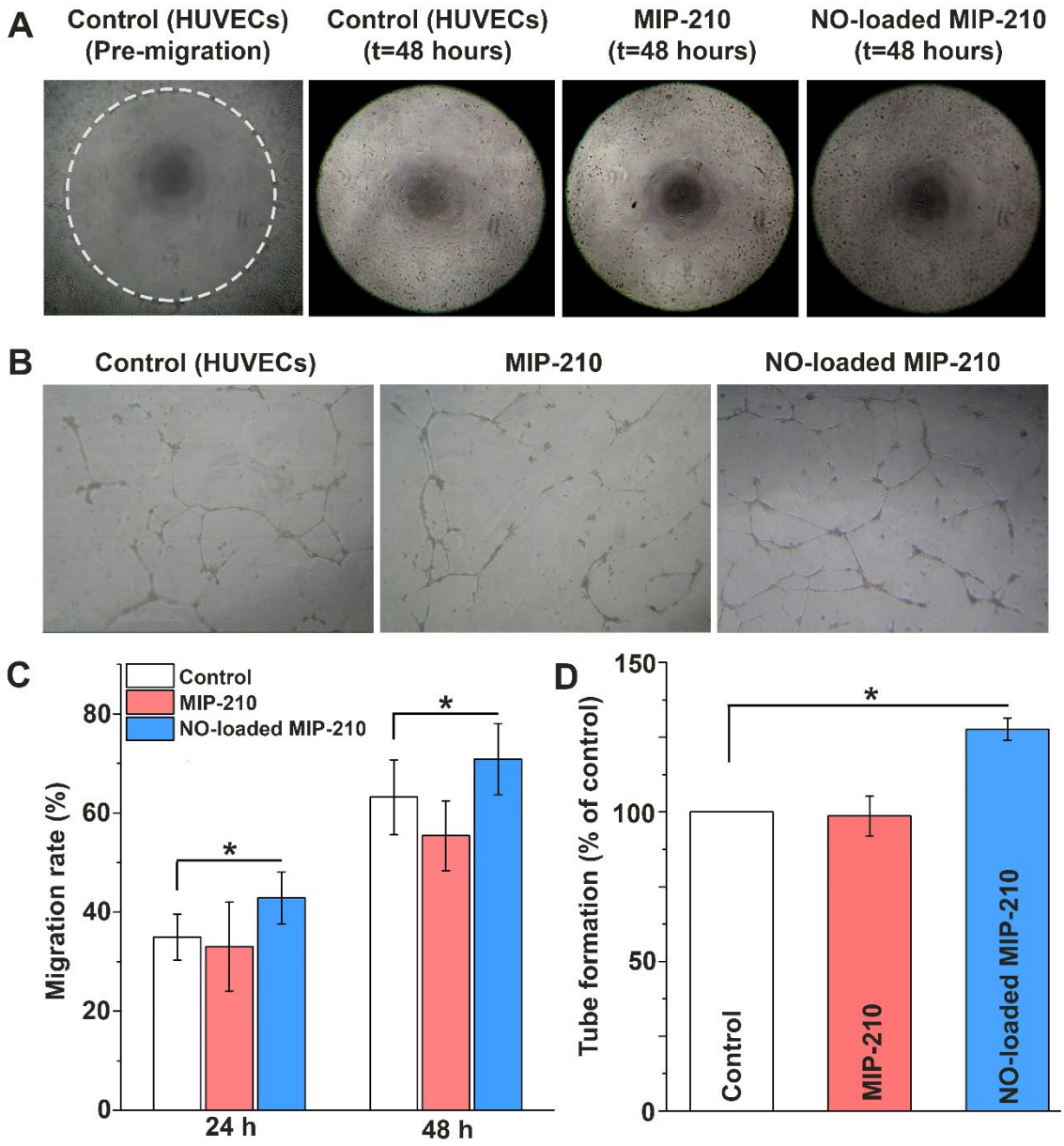

Figure 4. Effects of NO released by MIP-210(Fe) on HUVEC cells migration and on Geltrex tube-forming assay. A) Representative images of the Oris^{TM} cell migration assay in the pre-migration stage and after allowing cells to migrate in the presence (or not) of the MIP-210(Fe) (unloaded and loaded with NO) at the concentration of 11.75 $\mu g.mL^{-1}$. B) Example images of HUVEC tube formation after being treated with (or without) NO-releasing MIP-210(Fe) (11.75 $\mu g.mL^{-1}$) after 18 hours. C) HUVEC cells migration data after 24 and 48 hours. D) Quantification of tube formation (measured by the number of branches) after 18 hours. Graph values are expressed as mean ± SD ($n \geq 3$) and statistical differences were performed using unpaired t-test student (*$P<0.5$).

A previous report used a different cell line (HeLa cells) to demonstrate a similar improvement in the cell migration (+ 8.4±1.4% comparing with the control) induced by the NO released by a titanium carboxylate MOF (MIP-177)[5]. Moreover, a study presented by Zhang et al.[31] showed a NO-releasing system composed by a N-diazeniumdiolate modified copper-based MOF (HKUST-1) incorporated in polymeric nanofibers capable to significantly induce HUVEC proliferation, migration, and tube formation due to the gradual NO release (1.74 nmol L^{-1} h^{-1}) over more than 14 days[35]. However, copper-based MOFs and diazeniumdiolated-based NO releasing strategies are not likely to use (even if the donor is covalently bounded to the polymer matrix) since with the polymer degradation there will be the release of the toxic by-products.

The incorporation in a polymer support might indeed constitute a possible follow-up direction for MIP-210(Fe), in which poorly toxic composites based on this stable MOF might potentiate the NO release performance, assuring even longer periods and reduced side effects. In addition, the NO released concentration/duration might easily be tuned according to the therapeutic requirement, paving the way for continuous research in the development of NO delivery platforms capable to cover a wider range of working and providing an encouraging prospect for future practical clinical applications. In any case, the NO-releasing performance of the NO-loaded MIP-210(Fe) itself has convincingly proven an unprecedent release profile with no apparent toxicity for cells and a preliminary conception of its therapeutic potential.

References

1. Carpenter, A. W. & Schoenfisch, M. H. Nitric oxide release: Part II. Therapeutic applications. *Chem. Soc. Rev.* **41**, 3742–3752 (2012).
2. Palmer, R. M., Ferrige, A. G. & Moncada, S. Nitric oxide release accounts for the biological activity of endothelium-derived relaxing factor. *Nature* **327**, 524–526 (1987).
3. Ghimire, K., Altmann, H. M., Straub, A. C. & Isenberg, J. S. Nitric oxide: what's new to NO? *Am. J. Physiol. Cell Physiol.* **312**, C254–C262 (2017).
4. Carné-Sánchez, A., Carmona, F. J., Kim, C. & Furukawa, S. Porous materials as carriers of gasotransmitters towards gas biology and therapeutic applications. *Chem. Commun.* **56**, 9750–9766 (2020).
5. Pinto, R. V *et al.* Tuning Cellular Biological Functions Through the Controlled Release of NO from a Porous Ti-MOF. *Angew. Chemie Int. Ed.* **59**, 5135–5143 (2020).

6. Gregg, S. T., Yuan, Q., Morris, R. E. & Xiao, B. Functionalised solids delivering bioactive nitric oxide gas for therapeutic applications. *Mater. Today Commun.* **12**, 95–105 (2017).
7. Pant, J., Goudie, M. J., Brisbois, E. J. & Handa, H. 14 - Nitric oxide-releasing polyurethanes. in (eds. Cooper, S. L. & Guan, J. B. T.-A. in P. B.) 417–449 (Woodhead Publishing, 2016).
8. Ma, X., Lepoitevin, M. & Serre, C. Metal–organic frameworks towards bio-medical applications. *Mater. Chem. Front.* **5**, 5573–5594 (2021).
9. Eubank, J. F. *et al.* Porous, rigid metal(III)-carboxylate metal-organic frameworks for the delivery of nitric oxide. *APL Mater.* **2**, 124112 (2014).
10. Serre, C. *et al.* Synthesis, Structure and Properties of Related Microporous N,N‘-Piperazinebismethylenephosphonates of Aluminum and Titanium. *Chem. Mater.* **18**, 1451–1457 (2006).
11. Chakraborty, D. *et al.* A novel crystalline nanoporous iron phosphonate based metal–organic framework as an efficient anode material for lithium ion batteries. *New J. Chem.* **45**, 15458–15468 (2021).
12. Gagnon, K. J., Perry, H. P. & Clearfield, A. Conventional and Unconventional Metal–Organic Frameworks Based on Phosphonate Ligands: MOFs and UMOFs. *Chem. Rev.* **112**, 1034–1054 (2012).
13. Abu-Shandi, K., Winkler, H. & Janiak, C. Structure and Mössbauer Study of the First Mixed-Valence Iron Diphosphonate. *Zeitschrift für Anorg. und Allg. Chemie* **632**, 629–633 (2006).
14. Merrill, C. A. & Cheetham, A. K. Pillared Layered Structures Based upon M(III) Ethylene Diphosphonates: The Synthesis and Crystal Structures of MIII(H2O)(HO3P(CH2)2PO3) (M = Fe, Al, Ga). *Inorg. Chem.* **44**, 5273–5277 (2005).
15. Pinto, R. V. & Pinto, M. L. Chapter 14 - Nanoporous Materials: New Generation of Nitric Oxide Donors. in (eds. Morbidelli, L. & Bonavida, B. B. T.-T. A. of N. O. in C. and I. D.) 277–305 (Academic Press, 2019).
16. McKinlay, A. C. *et al.* Exceptional behavior over the whole adsorption-storage-delivery cycle for NO in porous metal organic frameworks. *J. Am. Chem. Soc.* **130**, 10440–10444 (2008).
17. Miller, S. R. *et al.* A rare example of a porous Ca-MOF for the controlled release of biologically active NO. *Chem. Commun.* **49**, 7773–7775 (2013).
18. McKinlay, A. C. *et al.* Nitric Oxide Adsorption and Delivery in Flexible MIL-88(Fe)

Metal–Organic Frameworks. *Chem. Mater.* **25**, 1592–1599 (2013).

19. Henkelman, G., Uberuaga, B. P. & Jónsson, H. A climbing image nudged elastic band method for finding saddle points and minimum energy paths. *J. Chem. Phys.* **113**, 9901–9904 (2000).
20. Hadjiivanov, K. I. Identification of Neutral and Charged N x O y Surface Species by IR Spectroscopy. *Catal. Rev.* **42**, 71–144 (2000).
21. Vasp TST tools. Available at: http://theory.cm.utexas.edu/vtsttools/.
22. Li, J., Banerjee, A., Pawlak, P. L., Brennessel, W. W. & Chavez, F. A. Highest Recorded N–O Stretching Frequency for 6-Coordinate {Fe-NO}7 Complexes: An Iron Nitrosyl Model for His3 Active Sites. *Inorg. Chem.* **53**, 5414–5416 (2014).
23. Wheatley, P. S. *et al.* NO-releasing zeolites and their antithrombotic properties. *J. Am. Chem. Soc.* **128**, 502–509 (2006).
24. Pinto, R. V. *et al.* New generation of nitric oxide-releasing porous materials: Assessment of their potential to regulate biological functions. *Nitric Oxide - Biol. Chem.* **90**, (2019).
25. Lin, Z. *et al.* Improved therapeutic nitric oxide delivery by microporous Cu-bearing titanosilicate. *Microporous Mesoporous Mater.* 111154 (2021) doi:https://doi.org/10.1016/j.micromeso.2021.111154.
26. Pinto, M. L., Pinto, R. V., Carvalho, S., Antunes, F. & Pires, J. Emerging nitric oxide and hydrogen sulphide releasing carriers for skin wound healing therapy. *ChemMedChem* **17**, (2022).
27. Baati, T. *et al.* In depth analysis of the in vivo toxicity of nanoparticles of porous iron(iii) metal–organic frameworks. *Chem. Sci.* **4**, 1597–1607 (2013).
28. Kaneko, T. *et al.* Effects of nicardipine on tube formation of bovine vascular endothelial cells in vitro. *Stroke* **23**, 1637–1642 (1992).
29. Neufeld, G., Cohen, T., Gengrinovitch, S. & Poltorak, Z. Vascular endothelial growth factor (VEGF) and its receptors. *FASEB J. Off. Publ. Fed. Am. Soc. Exp. Biol.* **13**, 9–22 (1999).
30. Morbidelli, L. & Ziche, S. D. and M. Role of Nitric Oxide in the Modulation of Angiogenesis. *Current Pharmaceutical Design* vol. 9 521–530 (2003).
31. Zhang, P. *et al.* Copper-Based Metal–Organic Framework as a Controllable Nitric Oxide-Releasing Vehicle for Enhanced Diabetic Wound Healing. *ACS Appl. Mater. Interfaces* **12**, 18319–18331 (2020).
32. Yang, T., Zelikin, A. N. & Chandrawati, R. Progress and Promise of Nitric Oxide-

Releasing Platforms. *Adv. Sci.* **5**, 1701043 (2018).

33. Duncan, M. J. *et al.* Antibacterial efficacy from NO-releasing MOF–polymer films. *Mater. Adv.* **1**, 2509–2519 (2020).
34. Zhan, R. *et al.* Nitric Oxide Enhances Keratinocyte Cell Migration by Regulating Rho GTPase via cGMP-PKG Signalling. *PLoS One* **10**, e0121551 (2015).
35. Chen, J. *et al.* MOFs-Based Nitric Oxide Therapy for Tendon Regeneration. *Nano-Micro Lett.* **13**, 23 (2020).
36. Feelisch, M., Kubitzek, D. & Werringloer, J. The Oxyhemoglobin Assay. in *Methods in Nitric Oxide Research* (eds. Feelisch, M. & Stamler, J. S.) 455–478 (John Wiley & Sons, Ltd, 1996).
37. Georget, V. & Baecker, V. ImageJ-macros: Wound Healing Tool.

Acknowledgements

CCC, PL, CYS, GM, ID, AT and CS acknowledge the financial support from the bilateral France China exchange program CaiYuanPei (ref. N° 38893VJ). RVP and MLP thanks the Fundação para a Ciência e a Tecnologia (FCT) for funding the projects UIDB/04028/2020 & UIDP/04028/2020 (CERENA), UIDB/00100/2020 and UIDP/00100/2020 (CQE) and LA/P/0056/2020 (IMS). RVP acknowledges Colégio de Química, University of Lisbon, for the BAD grantID. ID, AT and CS thank CNRS, ENS, ESPCI Paris and PSL university for financial and administrative support as well as the Paris region, through the DIM Respore priority project. Dr Debanjan Chakraborty is acknowledged for his assistance to construct the main figures.

Methods

Chemicals and Cells

All chemicals were purchased commercially and used as received without further purification. P-Xylylenebisphosphonic acid (H4mbpa), 99%, SIKEmia. Ferric chloride hexahydrate, 98%, Fisher. Ethanol absolute, ≥99%, Acros. MilliQ water, Millipore system, Sodium hydrosulphite (≥82% (RT)) and haemoglobin human lyophilized powder, Sigma-Aldrich, Nitric oxide gas (99.99%), Air Liquide.

HeLa cells were obtained from American Type Culture Collection (Manassas, VA, USA), HEKn cells from Thermo Fisher Scientific and HUVEC from Live Technologies. RPMI-1640 without L-glutamine, Corning Inc.; penicillin-streptomycin, L-glutamine, foetal bovine serum (FBS), trypsin (2.5%, without phenol red), Epilife medium with 60 µM calcium, human keratinocyte growth supplement kit, Medium 200 PRF, low serum growth supplement (LSGS), trypsin-EDTA (0.25% without phenol red), trypsin neutralizer solution and Geltrex™ LDEV-Free Reduced Growth Factor Basement Membrane Matrix were all purchased from Thermo Fisher Scientific.

Synthesis of MIP-210(Fe): $FeCl_3 \cdot 6H_2O$ (150 mg, 0.555 mmol) and H_4mbpa (111 mg, 0.417 mmol) were mixed with 5 mL of water in a 50 mL glass vial, sonicated for 15 minutes and then placed in an oven at 120 °C for 20 hours. The solid was washed with water and ethanol and the product was collected by centrifugation and dried under ambient atmosphere, leading to 120 mg of a bright yellow solid, which corresponds to a yield of 90 % based on ligand due to the excess of metal salt. This synthesis can also be performed in Teflon reactor in the same conditions to obtain uniform MIP-210(Fe) crystals (Fig. S1).
This synthesis can be scaled-up five times without any change of sample's quality. Besides, the same product can be obtained using different iron salt/ligand molar ratios (from 0.5 to 1.5) using similar conditions. It can also be obtained using any water volume between 5 to 10 mL and by adding formic acid or acetic acid as modulator.

Synthesis of MIP-210(Fe)-HT: A phase change happened when MIP-210(Fe) was heated at 120 °C under vacuum for 5 hours, leading to MIP-210(Fe)-HT.

Characterization of MIP-210(Fe). Powder X-ray diffraction (PXRD) data were recorded on a high-throughput Bruker D8 Advance diffractometer working on transmission mode and equipped with a focusing Göbel mirror producing CuKα radiation (λ=1.5418 Å) and a LynxEye detector. SEM-EDX characterization was performed with a FEI Magellan 400 scanning electron microscope. TGA data were collected on Mettler Toledo TGA/DSC 2, STAR System apparatus with a heating rate of 5 ºC / min. under oxygen or nitrogen flow. Crystal structure was obtained by single-crystal synchrotron diffraction data collected with micro-focused X-rays on the Proxima2A beamline (Synchrotron SOLEIL) using a suitable single crystal. Samples were analysed by FT-IR spectroscopy by using a Nicolet 6700 FTIR spectrometer equipped with a DTGS detector. Temperature dependent PXRD data were recorded with sample closely packed in quartz capillary on a PANalytical EMPYREAN

diffractometer with CuKα radiation (λ = 1.5418 Å) and equipped with an HTK-1200N (Anton Parr) high-temperature chamber and a GaliPIX3D detector.

Stability tests in biological conditions: Structural integrity of MIP-210(Fe) after being in contact with different supplemented cell culture media (RPMI-1640, Medium 200 and EpiLife – media used for HeLa, HUVEC and HEKn cells subculture, respectively) was evaluated under biological conditions (37 ºC, humidified atmosphere with 5 % CO_2). The concentration of material tested (450 µg/mL) was the same used to perform toxicity tests with these three cell lines. After 72 hours (maximum time of the accomplished cellular assays), iron concentration in each medium was quantified (after MOF removal by centrifugation) by inductive coupled plasma atomic emission spectroscopy (ICP-AES).

NO adsorption/desorption isotherms. MIP-210(Fe) (ca. 50 mg) was first outgassed for 12 hours at 120 ºC in vacuum, cooled up to 25 ºC and the adsorption isotherm was recorded after 80 kPa of NO being introduced to the system (equipment is set to only work under atmospheric pressure for safety reasons). NO adsorption and desorption isotherms were carried out using a gravimetric adsorption system (CI Electronics, Disbal microbalance), with 0.1 µg of precision, associated with a high vacuum system composed by turbomolecular and diaphragm pumps (Pfeiffer Vacuum). Over 72 hours, the sample weight was recorded every minute with both temperature and pressure controlled by using a water bath (Grant, GD120) and using a capacitance transducer (Pfeiffer Vacuum, CMR 262). Desorption of NO gas adsorbed was conducted in a similar manner by gradually evacuating the NO and maintaining the vacuum for 24 hours.

***In situ* IR characterization:** IR measurements were performed to follow the NO adsorption process using an IR *operando* setup comprising a reactor-cell associated to a high vacuum system (Pfeiffer). Sample was shaped in self-supported disks (16 mm diameter, 25 mg) and pretreated at different temperatures under vacuum (Figure S16). 1.3 kPa NO was then introduced in the cell and left in contact with the solid for 24 hours at room temperature. IR spectra were recorded periodically (128 scans, 4 cm^{-1} resolution) using a Nexus-Thermo Nicolet apparatus. After that period, NO was removed under secondary vacuum.

***In situ* PXRD characterization:** PXRD patterns of the pristine MIP-210(Fe), activated MIP-210(Fe) and NO-loaded MIP-210(Fe) were collected on a diffractometer on a Bruker D8 ADVANCE powder diffractometer with Linxeye-XE detector, with a Bragg Brentano geometry, using CuKα radiation (λ=1.5418 Å) at room temperature in capillaries. Briefly, pristine MIP-210(Fe) was inserted directly in a capillary while for the other conditions, MIP-210(Fe) was inserted in a capillary and activated under vacuum at 120 ºC for 12 hours. The capillary corresponding to the activated MOF was sealed and the material was kept inside the capillary under vacuum for XRD analysis. For the NO-loaded MIP-210(Fe) case, the NO was inserted inside the capillary after MOF activation and it was sealed with the NO inside for XRD analysis.

NO release kinetics. After pretreatment at 120 ºC for 12 hours, MIP-210(Fe) was exposed to 80 kPa NO in a glass vacuum cell for 72 hours. After the loading period, the non-adsorbed NO was evacuated, and the sample kept in helium atmosphere until application. NO released from MIP-210(Fe) in liquid phase was quantified using the oxyhemoglobin assay. Previously described by Feelisch *et al.*[36], this spectrophotometric technique allow the NO quantification in aerobic oxyhemoglobin solution by monitorization of the stoichiometric conversion by NO of oxyhemoglobin to methemoglobin. Briefly, MIP-210(Fe) was ground together with poly(tetrafluoroethylene) (PTFE) (25% wt), the mixture was pressed into pellets and loaded with NO in the same conditions as for the powder. Oxyhemoglobin solution was prepared by dissolving 20 mg of lyophilized human hemoglobin in 1 mL buffer solution and sodium dithionite was added for complete reduction of oxyhemoglobin. The solution was purified and desalted using a Sephadex G-25 column. For NO release quantification, the loaded MOF was placed in a quartz cuvette with 3 mL of oxyhemoglobin solution (1 µM) and spectra were recorded over time using a UV-Vis spectrophotometer (Genesys 10S, Thermo Scientific) until total oxyhemoglobin reduction. NO released was quantified according to the procedure also described by Feelisch *et al.*[36].

Molecular simulation: Periodic Density functional theory (DFT) calculations were performed to model the adsorption of NO in MIP-210(Fe) with Fe(III) saturated with terminal water molecule. These calculations considered a 2x1x1 supercell of the MIP-210(Fe)-293(K) crystal structure free of adsorbed water. Similar calculations were performed for the crystal structure determined for the MOF filled of water molecules.

Cell culture and cytotoxicity tests: HeLa cells (human cervical cancer cell line) were grown in RPMI-1640 medium supplemented with foetal bovine serum (10 % V/V), penicillin-streptomycin (100 UI.mL-1 and 100 µg.mL-1, respectively) and 2 mM glutamine. HEKn cells (epidermal keratinocytes isolated from neonatal foreskin) were cultivated in EpiLife® Medium supplemented with calcium, human keratinocyte growth supplement (HKGS) and an antibiotic/antimycotic solution of gentamicin and amphotericin B. HUVECs were cultured in Medium 200PRF supplemented with low serum growth supplement (LSGS). All cells were incubated at 37 °C in a humidified atmosphere with 5 % CO_2. Fresh medium was replaced every 1-2 days until the adequate confluency for subcultivation.
Viability/toxicity was estimated by the fluorometric resazurin assay. Cells were seeded in 96-well plates at the density of 7500 cells/well for 24 hours assays and 2500 or 5000 cells/well for 72 hours assays (HeLa or HUVEC/ HEKn cells, respectively). After 24 hours of incubation, the medium was replaced by fresh medium or by a suspension of medium with the sample at the desired concentration. Eight replicates were used for each condition. On the respective time, 10 µL per well of resazurin (final concentration of 10 µg/mL) was added and incubated for more 3 hours. Resazurin reduction was quantified by fluorescence (λ_{ex} = 530 nm, λ_{em} = 590 nm) in a Spectra Max Gemini EM reader from Molecular Devices. The fluorescence value of the supplemented medium was subtracted. Cell viability was calculated using the following equation:
Cell viability (%) = (F sample / F control) × 100 where F sample is the fluorescence of the cells incubated with samples and F control is the absorbance of the cells incubated without the sample.

HUVEC cells migration assay HUVEC cell migration was evaluated using the Oris™ Cell Migration Assay (Platypus technologies, LLC, Madison WI). In brief, HUVEC cells (50000 cells/well, from 2 to 5 passage) were seeded in a 96-well plate with "stopper" barriers in each well that create a central cell free detection zone. After incubation overnight, the stoppers were removed, allowing the cells to migrate into the detection zone, and the medium was replaced by fresh medium or by a medium containing unload or NO-loaded MIP-210(Fe) (11.75 µg.mL^{-1}). After 24 and 48 hours, each well was photographed using a microscope (Olympus, CK40) equipped with a digital camera (C4040; Olympus). A black mask with 96 prefabricated openings that precisely frame the central detection zone was attached to the bottom of the 96-well plate when the pictures were taken. The cell-free area within the detection zone was calculated using the ImageJ 1.50i software with a MRI wound healing tool [37]. The migration rate after 24 and 48 hours was calculated using the following equation (1):

$$\%\, migration\ rate = \frac{(Area_{pre-migration\ (t=0\ h)} - Area_{post-migration\ (t=x\ h)}}{Area_{pre-migration\ (t=0\ h)}} \cdot 100$$

The average percentage of migration rate and standard deviation of at least three independent assays (with ≥3 replicates each) were reported in the results. Unpaired student's t-test was used to assess significance with p-values < 0.05 considered statistically significant.

Endothelial cell tube formation assay: To confirm the angiogenic properties of the NO released by the MIP-210(Fe), tube formation assays were conducted using Geltrex™ as basement matrix and HUVEC cells (between 2-5 passage). Pre-frozen Geltrex™ (4ºC overnight in an ice bath) was added to a 24-well plate (95 µL/well) and the precoated plate was incubated for 30 minutes at 37 ºC to allow the gel to solidify. Then, HUVEC cells (225000 cells mL^{-1}) were diluted in supplemented Medium 200PRF in the absence or presence of the unloaded or NO-loaded MIP-210(Fe) and seeded in each gel-coated well (85500 cells/well). The plate was incubated at 37 ºC, 5% CO_2 for 18 hours. After that period, the tube network formation was observed

and photographed with a microscope (Olympus, CK40) equipped with a digital camera (C4040; Olympus). The number of microvascular branches formed was quantified using ImageJ 1.50i software with the angiogenesis analyser plugin. Quantification data presented is expressed in comparison with the control. Three independent assays with 3 replicates each were performed for each condition. Unpaired student's t-test was used to assess the statistical significance.